Measurement 257 (2026) 118766

Contents lists available at ScienceDirect

Measurement

journal homepage: www.elsevier.com/locate/measurement

Advanced respiratory disease monitoring: a machine learning driven software defined radios approach for accurate respiratory rate☆

Malik Muhammad Arslan [a], Xiaodong Yang [a,*], Lei Guan [a], Nan Zhao [a], Tao Cui [a], Mubashir Rehman [b], Abbas Ali Shah [a], Muhammad Bilal Khan [b], Syed Aziz Shah [c], Qammer H. Abbasi [d,e]

[a] Key Laboratory of High Speed Circuit Design and EMC, Ministry of Education, School of Electronic Engineering, Xidian University, Xi'an, Shaanxi 710071, China
[b] Department of Electrical and Computer Engineering, COMSATS University Islamabad, Attock Campus, 43600, Pakistan
[c] Research Centre for Intelligent Healthcare, Coventry University, Coventry CV1 5FB, UK
[d] James Watt School of Engineering, University of Glasgow, Glasgow G12 8QQ, UK
[e] College of Engineering, Abu Dhabi University, UAE

ARTICLE INFO

Keywords:
Biomedical signal processing
Electromagnetic sensing
Machine learning
Non-invasive monitoring
Respiratory disease management
RF sensing
SDR technology
USRP

ABSTRACT

Respiratory disease management has become a critical area of focus, necessitating innovative solutions for continuous and non-invasive monitoring. Human respiratory patterns, which reflect the rate, depth, and rhythm of breathing, are vital indicators of an individual's physical and mental health. Effective monitoring of these patterns can aid in diagnosing related disorders and, significantly improving patient care. This study proposes a contactless respiratory pattern recognition system that utilizes an advanced radio frequency (RF) sensing framework combined with smart software-defined radio (SDR) technology and machine learning algorithms. The system ensures precise measurement and recognition of the respiratory patterns. Initially, data-preprocessing techniques were developed to capture the time-domain respiratory signals from the received data accurately. Additionally, a method based on Fast Fourier Transform (FFT) was employed to detect abnormal respiratory rates. Subsequently, various machine learning algorithms were applied, with the Medium Tree algorithm proving to be highly effective. The experimental results indicate that the system can accurately identify multiple respiratory cycles, including eupnea, tachypnea, and bradypnea, achieving an accuracy of 89.8 % in scenarios involving up to five individuals. The Area Under the Receiver Operating Characteristic (AUROC) scores demonstrated the superior performance of the Medium Tree model (98.5 to 89.8 %) compared to Linear SVM (97.4 to 85.3 %), Linear Discriminant (94.6 to 87.6 %), Naive Bayes (98.3 %), and Coarse KNN (96.4 %), with a paired *t*-test ($p = 0.0238$) confirming its significant advantage over the Linear Discriminant model. The system performance was validated in diverse indoor environments, thereby demonstrating its robustness and reliability. The proposed contactless respiratory pattern recognition system demonstrates the feasibility of long-term continuous respiratory monitoring.

1. Introduction

Respiration is a fundamental biological function critical for sustaining normal physiological processes in the human body [1]. It is profoundly linked to overall physical and mental well-being [2,3]. Respiration rate and pattern serve as reliable indicators of an individual's health condition [4], necessitating improved diagnostic methods.

Normal respiration is characterized by natural and sequential expansion and contraction of the abdominal and chest muscles [5]. The eupneic breathing pattern is steady in terms of pace, depth, and frequency [6]. Healthy adults typically have a respiration rate (RR) of 12–20 breaths per minute (bpm), whereas infants and children breathe more rapidly than adults do. Various medical conditions can alter respiration patterns, affecting their rate, depth, and regularity [7]. Bradypnea, defined as a respiratory rate below 12 bpm, is often

☆ This article is part of a special issue entitled: 'Medical Measurement' published in Measurement.

* Corresponding author at: No. 2 South Taibai Road, Xidian University, Xi'an, Shaanxi 710071, China.
E-mail address: xdyang@xidian.edu.cn (X. Yang).

https://doi.org/10.1016/j.measurement.2025.118766
Received 12 December 2024; Received in revised form 12 August 2025; Accepted 19 August 2025
Available online 19 August 2025
0263-2241/

associated with cardiovascular disease, thyroid dysfunction, and obstructive sleep apnea [8].Tachypnea, characterized by a respiration rate exceeding 20 bpm, can be caused by conditions such as sepsis, acidosis, and respiratory issues [9]. Patients with encephalitis often exhibit Biot's breathing, an irregular pattern with equal-depth breathing, and periods of apnea [10]. Cheyne-Stokes breathing, marked by recurrent crescendo-decrescendo patterns and central apnea or hypopnea, is common in individuals with heart failure [11]. Additionally, children with autism spectrum disorders may show Biot's and Cheyne-Stokes breathing patterns [12], whereas Kussmaul respiration, characterized by deep, rapid, and labored breathing, is linked to acute metabolic acidosis, which is commonly observed in diabetic ketoacidosis [13].

Accurately detecting typical respiratory patterns, particularly during sleep, is challenging without hospitalization or specialized respiratory observation facilities. Traditionally, the evaluation of irregular respiration patterns has depended on skilled professionals, leading to missed opportunities for diagnosing serious illnesses or providing life-saving therapy when specialists are unavailable. Hence, there is a compelling need for a system that can discreetly and continuously monitor and identify typical respiration cycles in various scenarios. Conventional techniques for detecting respiration patterns require individuals to use specialized equipment, which limits the feasibility of indoor health monitoring, particularly for the elderly and patients with dermatological allergies and injuries [14]. These methods rely heavily on skilled professionals, limiting timely diagnosis and intervention in scenarios in which specialized expertise is unavailable.

Recent advances in non-contact respiratory monitoring offer a promising solution to address the limitations of traditional approaches [15,16]. Non-invasive respiratory monitoring techniques are preferred for long-term observation, and the demand for contactless sensing technologies has significantly increased owing to the COVID-19 pandemic [17,18]. Researchers have investigated a range of non-contact methods for detecting respiration, including radar technologies such as frequency-modulated continuous wave radar [19], laser Doppler vibrometer-enabled sensing [20],Continuous wave Doppler radar [17,21,22], ultra-wideband radar [23], Wi-Fi-based methods [24–26], and camera-based approaches [27]. In addition, the SDR has been employed to monitor respiratory signals. Although many studies have focused on measuring respiratory rates using RF signals, there is a paucity of research on breathing pattern classification [28]. For instance, a specially designed 2.4-GHz Doppler radar system attained a classification accuracy of 94.7 % in identifying six distinct breathing patterns through the application of a support vector machine (SVM) classifier.[29]. Another approach using a 1D convolutional neural network (1D CNN) identified four distinct breathing rhythms captured by UWB radar, achieving an average accuracy of 95.8 % [30]. A system utilizing Universal Software Radio Peripheral (USRP) and Deep Multilayer Perceptron (DMLP) classification achieved an accuracy rate as high as 99 % in identifying and classifying six different breathing pattern [31]. Similarly, a classifier based on random forests used impulse radio ultra-wideband (IR-UWB) radar to categorize four distinct respiration patterns, with an overall accuracy of 90 % [32].

In addition to radar-based techniques, Wi-Fi-based Channel State Information (CSI) methods have gained popularity for extracting features in respiratory monitoring [33,34]. Numerous studies have developed CSI applications for purposes such as human identification, monitoring respiratory illnesses in single individuals, and detecting indoor human presence and respiratory signals [35]. According to the literature, Wi-Fi signals can detect and distinguish even slight chest movements [36].The camera-based approach for respiratory sensing primarily depends on video-based methods for extracting respiratory rhythms using consumer-grade red–green–blue (RGB) cameras and computer vision algorithms [37].

This method involves detecting and tracking a custom pattern on the thorax of a subject to compute positional changes over time, thereby extracting respiratory signals. However, RGB cameras are restricted to controlled environments and stationary subjects because of their high sensitivity to non-respiratory movements and variations in environmental lighting, which can affect data accuracy. They are also ineffective at night in the absence of an active light sources [38]. Despite these advancements, the existing methods still face critical limitations. Radar and Wi-Fi-based CSI systems often struggle in dynamic, multi-person scenarios, suffering substantial performance degradation due to overlapping signals and environmental noise. Similarly, camera-based solutions fail in low-light or motion-intensive scenarios. Thus, there remains a critical gap in reliable, multi-person respiratory pattern classification under realistic and, variable conditions.

The SDR approach utilizes purpose-built hardware specifically engineered for accurate sensing and monitoring of respiratory rates. Systems such as WiSee utilize USRP to identify Doppler shifts in wireless signals, thereby enabling the detection of breathing rate activities with an accuracy of up to 94 % [39].To address this significant gap, our study introduces a novel, contactless respiratory monitoring system capable of reliably classifying multiple respiratory patterns (eupnea, bradypnea, and tachypnea) simultaneously for up to five individuals. Our proposed framework utilizes Software-Defined Radio (SDR) technology, employing precise RF-based sensing coupled with computationally optimized signal processing and machine learning. By combining FFT-based frequency-domain analysis with a rigorously optimized Medium Tree classifier, our approach achieves state-of-the-art accuracy (single-subject to multi-subject) and computational efficiency, significantly outperforming existing radar, CSI, and camera-based methods. This combination of high throughput, robustness in noisy environments, and practical scalability sets our system apart from those of previous studies. Fig. 1. depicts the components of the proposed system, including data collection, data preprocessing, and a multi-person respiration pattern identification module. The significant contributions of this study are as follows.:

- We present a contactless system capable of simultaneously monitoring and classifying respiratory patterns (eupnea, bradypnea, and tachypnea) for up to five individuals using SDR and RF sensing, achieving state-of-the-art accuracy (89.8 % for five subjects). This addresses a critical gap in prior studies that are limited to single-subject scenarios or that suffer from performance degradation in multi-person settings.
- The proposed framework combines FFT-based frequency-domain analysis with a machine learning architecture, including a Medium Tree classifier optimized for respiratory signal separation. Experimental validation demonstrates statistically significant improvements over established benchmarks (Linear SVM, Naive Bayes), achieving AUROC scores of 98.5 % (single-subject) to 89.8 % (five-subject) with $p = 0.0238$ significance in paired t-tests.
- This work introduces a novel real-time respiratory monitoring framework that simultaneously achieves: clinical-grade accuracy at 10,000 observations/second via computationally optimized signal processing that outperforms deep learning in throughput (12 $\times$) and memory efficiency (83 %), enabling practical clinical deployment.
- Clinically viable operation across diverse environments, maintaining robust performance where camera-based systems fail (under variable lighting) and Wi-Fi CSI methods degrade (under noisy conditions), which is critical for reliable deployment in both clinical and home settings.

2. Preliminaries of RF-based respiration sensing with SDR

An RF-based SDR system was developed in this study for the continuous detection of respiration rates in multi-person scenarios, as shown in Fig. 1, using two units, each equipped with a single antenna for both transmitting and receiving, thereby enhancing the signal reliability and overall performance. When an individual is within the range of the

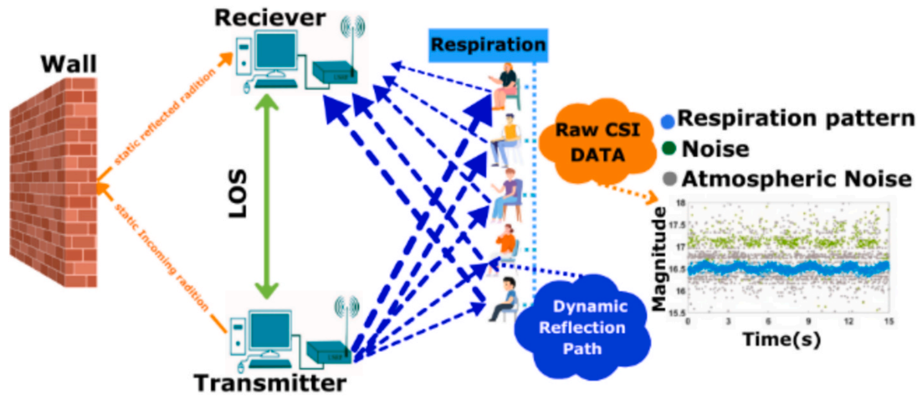

Fig. 1. Illustration of a multi-human respiratory model: RF units, signal processing, and classification modules.

system, their respiratory activity causes the RF signal to be reflected off the body, resulting in variations in CSI captured at the receiver. These variations contain two crucial types of information pertinent to respiratory activity. Initially, time-domain CSI amplitude data were collected by the system, capturing the entire inspiration and expiration process over a period. The respiratory patterns for eupnea, bradypnea, and tachypnea are depicted in Fig. 2(a–c), revealing distinct variations in the breathing rates. Subsequently, the respiration pattern was identified by counting breaths within a specific time frame, demonstrating its ability to accurately monitor breathing.

frequency. In Fig. 2(a), eight cycles were counted over 30 s(s), leading to a respiration rate of 16 bpm when scaled to a 1-minute duration (8 cycles $\times$ (60 s/30 s) = 16 bpm), which is characteristic of eupneic breathing. Similarly, Fig. 2(b) and 2(c) show respiration rates of 8 bpm (4 cycles) and 24 bpm (12 cycles) for bradypnea and tachypnea breathing, respectively. While time-domain CSI amplitude data are effective for detecting respiration rates in single-person scenarios, they pose challenges in multi-person scenarios owing to the interference from multiple independent chest movements.

To address this issue, the time-domain CSI data underwent FFT, converting it into the frequency domain, thereby improving the capacity of the system to analyze and interpret the CSI amplitude data.FFT isolates the frequency components of the signal, facilitating the identification of distinct respiration patterns. As shown in Fig. 3(a-c), the FFT application yielded prominent frequency peaks corresponding to the respiration rates. Respiration rate was computed using the following equation (1):

$$Respirationrate(bpm) = \left(\frac{numberofpeaks}{obseravtiontime(30sec)}\right)*60 \tag{1}$$

Here, number of peaks refers to the peaks detected in 30 s detailed in Table 1. As illustrated in Fig. 3 (a-c), the peak frequency associated with eupnea breathing exceeds that of bradypnea breathing but is lower than that of tachypnea breathing; In scenarios involving multiple individuals, each person's respiration rate produces a unique frequency peak, allowing the system to distinguish between different respiratory activities. For instance, in a two-person scenario, two significant frequency peaks were observed, corresponding to the individual respiration patterns.

3. Methodology

The SDR-based respiratory signal acquisition component, CSI preprocessing and respiratory pattern inference phase, and machine learning-based respiratory pattern classification framework are depicted in Fig. 4, outlining the designed system architecture, with each module described and elaborated upon in subsequent sections.

3.1. SDR-based respiratory signal acquisition

The SDR-based system for respiratory signal acquisition includes a transmitter, wireless channel, and receiver, each with a laptop and an NI-2922 USRP device.The laptop runs the SDR software in LabVIEW, whereas the NI-2922 USRP (with an omnidirectional antenna) manages RF functions. Initially, the respiratory signals were acquired. The transmitter synthesizes random bitstreams and, encodes them into concurrent sequences. These sequences were subsequently modulated using Quadrature Amplitude Modulation (QAM), followed by the insertion of training symbols and null values to create the OFDM structure. An inverse FFT reverts frequency-domain data back to the time domain, after which a cyclic prefix (CP) is appended by duplicating the final 25 % of the signal points at the beginning of each frame;which CP helps mitigate timing and frequency errors, and the data are subsequently transmitted to the USRP device at 20MS/s through a gigabit Ethernet connection.

The signal underwent digital up-conversion (DUC) to elevate its frequency to 400 MS/s, followed by digital-to-analog conversion, which then passed through a baseline filter with a 20 MHz bandwidth, combined with the designated carrier frequency, was amplified for gain adjustment, and was ultimately transmitted by the USRP unit via an omnidirectional antenna. The system detects respiratory-induced

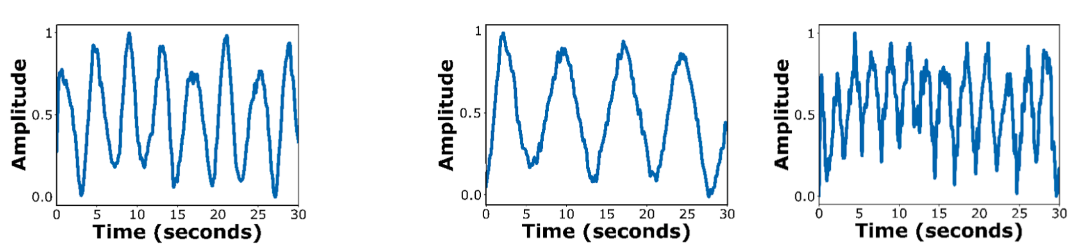

(a) Eupnea Respiration rate (b) Bradypnea respiration rate (c) Tachypnea respiration rate

Fig. 2. Respiration rate analysis using frequency-domain CSI amplitude signals: (a) Eupnea (16 bpm, 8 cycles/30 s), (b) Bradypnea (8 bpm, 4 cycles/30 s), (c) Tachypnea (24 bpm, 12 cycles/30 s).

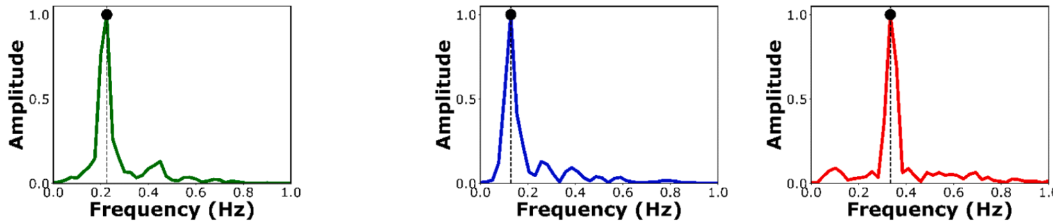

(a) Eupnea respiration rate (b) Bradypnea respiration rate (c) Tachypnea respiration rate

Fig. 3. FFT frequency-domain analysis: (a) Eupnea (0.266 Hz), (b) Bradypnea (0.133 Hz), (c) Tachypnea (0.4 Hz).

Table 1
OFDM based respiration rate.

Respiration Type	Number of Peaks	Time (t)	Frequency (f)	Respiration Rate
Eupnea	8	30 s	8/30 = 0.266 Hz	60*0.26≈16 bpm
Bradypnea	4	30 s	4/30 = 0.133 Hz	60*0.13≈8 bpm
Tachypnea	12	30 s	12/30 = 0.4 Hz	60*0.4≈24 bpm

Note: Respiration rates calculated by scaling 30-second peak counts to breaths/minute (×60).

Channel State Information (CSI) variations in indoor wireless environments.

These CSI fluctuations aid in estimating respiratory rates in a multi-person environment. This study determines the channel frequency response (CFR) of wireless CSI using wireless CSI through the application of Eq. (2).

$$G(n) = \frac{B(n)}{A(n)} \tag{2}$$

In this scenario, CFR is represented as $G(n)$, while $A(n)$ and $B(n)$ denote the transmitted and received frequency-domain signals, respectively, Given that $G(n)$ is a composite parameter, its amplitude response can be determined using Eq. (3) as follows:

$$|G(n)| = \sqrt{{G_{Re}}^2 + {G_{Im}}^2} \tag{3}$$

Furthermore, G_{RE} and G_{Im} Depict the actual and hypothetical components of the CFR respectively, with the amplitude data across multiple OFDM Frames for a single experimental trial M provided by Eq. (4).

$$|M| = \begin{bmatrix} |G(e^{j\omega})|_{1,1} & |G(e^{j\omega})|_{1,2} & \cdots & |G(e^{j\omega})|_{1,P} \\ |G(e^{j\omega})|_{2,1} & |G(e^{j\omega})|_{2,2} & \cdots & |G(e^{j\omega})|_{2,P} \\ \vdots & \vdots & \cdots & \vdots \\ |G(e^{j\omega})|_{N,1} & |G(e^{j\omega})|_{N,2} & \cdots & |G(e^{j\omega})|_{N,P} \end{bmatrix} \tag{4}$$

In this context, N represents the complete set of OFDM subcarriers, P signifies the packets collected during an individual measurement at the USRP receiver unit, the signal is first captured by an all-directional antenna array, amplified using a low-noise preamp (LNA) and a buffer amplifier to increase gain and minimize noise, It is then processed with direct conversion receivers (DCRs) to produce a baseband intricate signal. This signal is subsequently filtered through a 20 MHz bandwidth low-pass filter (LPF), sampled using a 2-channel analogue-to-digital converter (ADC) at 100 MS/s, and processed by digital down-converters (DDCs) that mix, filter, and decimate the signal at a user-defined rate, before finally being transmitted to the host laptop via a gigabit Ethernet connection at speeds of up to 20 MS/s. utilizing Van de Beek's algorithm [40], channel estimation (CE) errors at the receiver's host laptop were eliminated, and the time and frequency offsets were corrected. Subsequently, the FFT converts the temporal signal into the spectral domain, where the amplitude response is analyzed to determine the respiratory rate.

3.2. SDR-based respiratory CSI preprocessing and respiratory pattern inference module

To optimize the analysis, the raw data obtained from the SDR-based respiratory signal acquisition blocks were processed using a signal preprocessing module to extract crucial details and minimize noise. Although the OFDM signal at the receiver includes both the amplitude and phase information, only the amplitude is used to detect the respiratory rate. Preprocessing involves several steps, which are detailed as belows.

3.2.1. Subcarrier Selection

A set of 256 OFDM subcarriers was captured at the receiver to monitor respiratory activity, and the analysis indicated that each subcarrier had a distinct amplitude response, reflecting varying sensitivities to different respiratory dynamics. Therefore, the subcarriers with minimal sensitivity were discarded by calculating the variance for each subcarrier and subsequently removing those with the lowest variance.

3.2.2. Removing Outliers

Following the selection of essential subcarriers, a wavelet transform

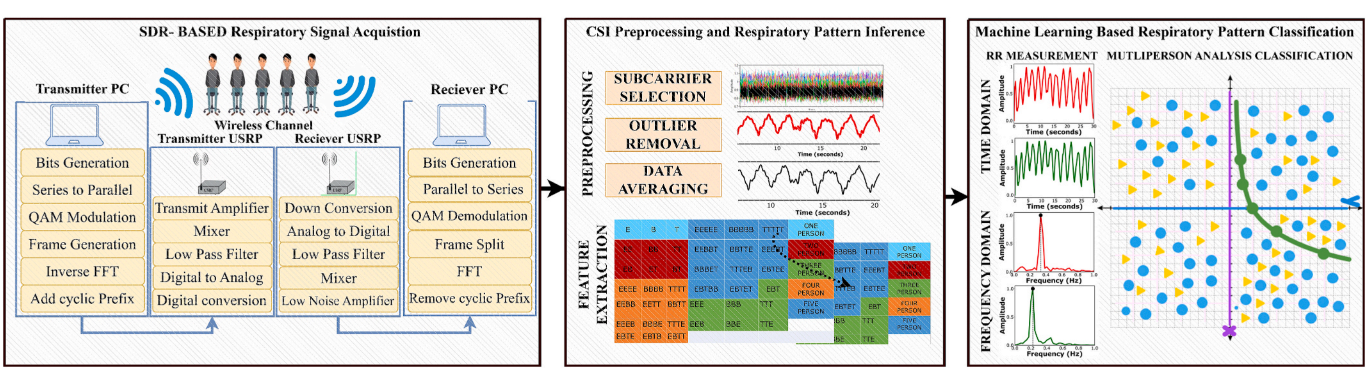

Fig. 4. System Architecture of the SDR-based respiratory monitoring platform.

is utilized to remove anomalies from the raw dataset while preserving distinct transitions using Stein's Unbiased Risk Estimate (SURE) thresholding with the adjusted noise option applied to the detail coefficients for wavelet analysis.

3.2.3. Data Averaging

For data averaging or refinement, an 8-sample window moving average filter was applied to smooth the data and suppress high-frequency noise unrelated to breathing activity, allowing for the easy identification of abnormal respiratory rates after these preprocessing steps.

3.2.4. Feature Extraction

For the subsequent preprocessing, the data represent the CSI corresponding to different respiratory rates. Feature extraction was performed to obtain meaningful information from the dataset. This step is crucial in classification methodologies because it reduces computational complexity by decreasing data dimensionality [41]. In this study, statistical features were extracted, and the data dimensions were reduced after feature extraction [42]. The mean and standard deviation capture breathing regularity, whereas kurtosis and skewness detect deviations from normal patterns. Entropy measures signal complexity and is, particularly useful in identifying pathological breathing.The peak-to-peak value and maximum frequency provide complementary information regarding amplitude and rate variations. These features collectively provide a comprehensive representation of respiratory dynamics while maintaining computational efficiency for real-time processing. The details of these features selection criteria and validation are presented in Table 2.

Our respiratory rate classification employed a three-stage frequency-domain validation process. First, we identified candidate peaks in the power spectral density (PSD) that exceeded the 85th percentile of the normalized energy (0–1 scale). Second, we rejected harmonic artifacts by discarding subpeaks at 1/2 or 1/4 frequencies when their power ratio exceeds 0.3 relative to the primary peak. Third, we validated against clinical respiratory ranges as described in Table 1, to ensure physiological plausibility. This approach significantly reduces harmonic interference while maintaining sensitivity to true respiratory signals.

3.2.5. Noise and interference Mitigation

The system addresses real-world challenges using the following approach: Adaptive noise floor estimation is used to minimize the impact of noise in the system. which is given by Eq. (5)

$$\sigma^2_{noise}[k] = 0.25 \bullet |v[k] - u[k]|^2 + 0.75 \bullet \sigma^2_{noise} \tag{5}$$

where $v[k]$ represents the CSI amplitude at subcarrier k, $u[k]$ is the moving average (calculated using a 5-sample window), and subcarriers with a Signal-to-Noise Ratio (SNR) of less than 8 dB are excluded. Spectral kurtosis is used for interference suppression. The criterion for interference detection is given by Eq. (6):

$$K(f) = \frac{E\left[\left|S(f)^4\right|\right]}{\left(E\left[\left|S(f)^2\right|\right]^2\right)} - 3 \tag{6}$$

If$K(f) > 3.5$, a notch filter is activated to suppress interference. $E\left[\left|S(f)^2\right|\right]$ is the signal power at frequency f and $E\left[\left|S(f)^4\right|\right]$ is a is a -higher-order statistic sensitive to interference. Motion artifact removal is achieved through Independent Component Analysis (ICA) to separate respiratory components, followed by Kalman filtering for improved accuracy represented by Eq. (7):

$$\hat{x}_t = F_t\hat{x}_{t-1} + K_t(z_t - H_tF_t\hat{x}_{t-1}) \tag{7}$$

where $\hat{x}_t$ is the estimate of the state at time t, F_t is the state transition matrix, K_t is the Kalman gain, z_t is the measurement at time t, and H_t is the observation matrix.The separated respiratory signals (e.g., in Fig. 7) may exhibit minor temporal offsets due to the convergence behavior of ICA/BSS algorithms. These misalignments arise because each component is extracted independently, but they do not affect the respiratory rate estimation, which relies on the frequency-domain periodicity (Section 5.1.2). Time-domain normalization was applied during preprocessing to ensure consistent feature extraction.

3.3. Machine learning-based respiratory pattern classification framework

The final section classifies abnormal respiratory patterns using five machine learning (ML) algorithms, including the training, validation, and testing stages within this classification framework. These algorithms can identify abnormal respiratory pattern in multi-person settings, and their efficacy depends on the dataset size and composition. each carefully selected and optimized to process the unique characteristics of RF-derived respiratory signals. The methodology followed a rigorous pipeline from feature extraction to model training, ensuring robust performance across varying subject counts.The input data underwent comprehensive preprocessing before model training. We apply standard scaling (z-score normalization) to all eight statistical features to ensure equal contributions during training. Feature selection was performed using ANOVA F-tests ($p < 0.01$) to retain only the most discriminative features for the respiratory pattern classification.

3.3.1. Algorithm configurations and training protocol

This section outlines the configurations and protocols for training machine learning models for respiratory pattern classification, focusing on performance optimization, parameter tuning, regularization, and evaluation to ensure robust classification across various patterns.

Table 2
Statistical parameter.

Sr.#	Reference	Parameter	Formulation	Significance
1	[10,28]	Mean	$\overline{x} = \frac{\sum_{i=1}^{n} x_i}{n}$	Average amplitude of the signal
2	[28,43]	Standard deviation	$x_{SD} = \sqrt{\frac{1}{n}\sum_{i=1}^{n}(x_i - \overline{x})^2}$	Variability in signal amplitude.
3	[20]	RMS	$x_{RMS} = \sqrt[2]{\frac{1}{n}\sum_{i=1}^{n} {x_i}^2}$	Overall power of the signal.
4	[6]	Kurtosis	$x_{Kur} = \frac{\frac{1}{n}\sum_{i=1}^{n}(\lvert x_i \rvert - \overline{x})^4}{{x_{SD}}^4}$	Sharpness or flatness of waveform.
5	[2]	Skewness	$x_{Skew} = \frac{\frac{1}{n}\sum_{i=1}^{n}(\lvert x_i \rvert - \overline{x})^3}{{x_{SD}}^3}$	Asymmetry of the waveform.
6	[42]	Entropy	$x_{Ent} = \sum_{i=-n}^{n} hist(x_i)\, ln_2(hist(x_i))$	Complexity and randomness.
7	[29]	Peak-to peak value	$x_{p-p} = x_{max} - x_{min}$	Amplitude range of signal
8	[16]	Maximum Frequency	$X_{fmax} = Max(FFT(x))$	Dominant frequency of signal

Medium Tree Classifier
We implement a decision tree a balanced depth to handle the complexity of respiratory patterns while preventing overfitting. The tree uses the Gini impurity for node splitting, with parameters optimized through a Bayesian search. The tree configuration included a maximum depth of 20 nodes, a minimum of 8 samples per leaf, and a minimum impurity decrease of 0.01. To simplify the final model and avoid excessive complexity, cost-complexity pruning was applied at $\alpha = 0.01$
Linear Discriminant Analysis (LDA)
LDA is configured to maximize the separation between the three respiratory pattern classes. The algorithm computes the between-class and within-class scatter matrices. Regularization was applied with $\lambda = 1 \times 10^{-4}$ to ensure numerical stability during matrix inversion and prevent issues caused by small or singular matrices.
Gaussian Naive Bayes
This probabilistic classifier assumes conditional independence between features given the class. We implement Gaussian likelihood functions with a smoothing parameter $\varepsilon = 1 \times 10^{-9}$ to handle zero variances. Additionally, logarithmic transformations are applied to probabilities prevent numerical underflow during multiplication and division of very small values.
Linear Support Vector Machine (SVM)
The SVM was configured with a linear kernel and L_2 regularization (C = 1.0). We employed Sequential Minimal Optimization (SMO) for efficient training, with a convergence tolerance of 1×10^{-3}. The algorithm seeks the optimal hyperplane that maximizes the margin between different respiratory pattern classes, ensuring a robust and accurate classification.
Coarse k-Nearest Neighbors (K-NN)
The k-NN implementation uses the Euclidean distance metric with k = 10 neighbors. A Ball Tree data structure with a leaf size of 30 was used to accelerate neighbor searches in the feature space. Voting weights are assigned based on the inverse distance, providing more influence to closer neighbors in the decision-making process.

3.3.2. Model training and validation

Following the algorithm configurations and training protocols outlined earlier, the training protocol employed a stratified 70–15-15 split for the training, validation, and test sets, respectively. Hyperparameter optimization was conducted using Bayesian methods with 30 iterations. Nested 5 × 5 cross-validation was applied to ensure reliable performance estimates. All implementations utilize float32 precision for efficient computation on an Intel i7-10750H platform with 16 GB RAM. Parallel processing is employed where applicable, using Joblib for efficient implementation of parallel tasks and OpenMP for tree construction. We implemented several safeguards against overfitting: (1) participant-wise separation between training and test sets, (2) L2 regularization ($\lambda = 0.01$) on all trainable parameters, and (3) early stopping based on the 15 % validation set.The entire pipeline is optimized to maintain computational efficiency while handling high-dimensional RF signal data, with a particular focus on real-time processing requirements for respiratory monitoring applications.

3.3.3. Algorithm selection Justification

To ensure that our algorithm selection was comprehensive, we evaluated four additional state-of-the-art approaches: Random Forest (100 trees, max_depth = 15), SVM with RBF kernel (C = 1.0, gamma='scale'), XGBoost (learning_rate = 0.1), and a Multi-layer perceptron (2 hidden layers). These were optimized using the same Bayesian hyperparameter search and validation protocol described in Section 3.3.2.

4. Experimental setup

4.1. Data collection

The experimental configuration for acquiring the respiratory rate data involved a pair of USRP devices connected to laptops, as depicted in Fig. 5. USRP devices, equipped with antennas that transmit and receive signals omnidirectionally, can identify irregular human respiratory rates under line-of-sight (LOS) and non-LOS (NLOS) conditions, demonstrating their potential for a range of health monitoring applications. The transmitter and receiver devices, each comprising a laptop connected to a USRP via an Ethernet cable, produce OFDM subcarrier data and preprocessed and classified raw respiratory signals, respectively. In all experiments, the Tx and Rx devices were positioned apart and aligned with the midsection of the human body to effectively capture breathing signals, showcasing a precise setup for respiratory monitoring.

To evaluate the real-world performance, we conducted tests under varying conditions including: (1) non-line-of-sight configurations with furniture obstructions, (2) environments with competing 2.4 GHz and 5 GHz WiFi signals, and (3) scenarios with intermittent movement in the

Table 3
Subjects' Characteristics.

Variables	Mean	Min-Max
Height (cm)	166	139–177
Weight (lbs)	154	125–180
Age (Years)	28	20–36
Body Mass Index	25	17–35

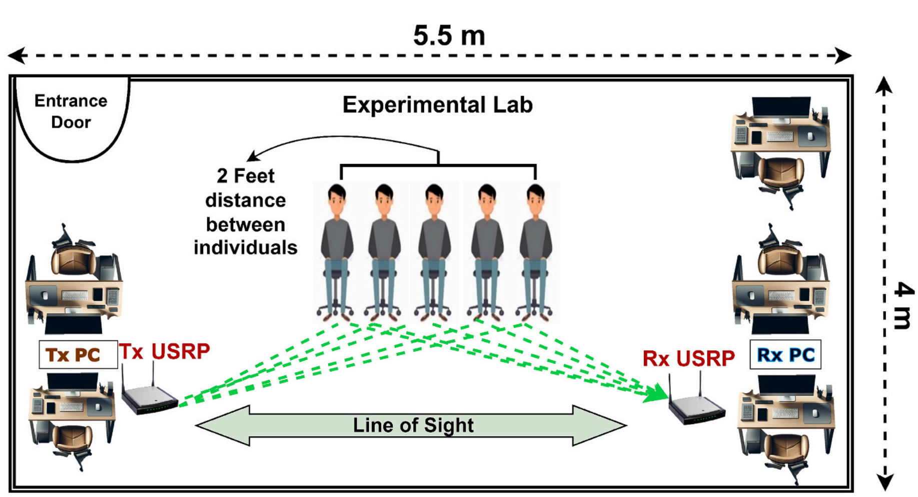

Fig. 5. Systematic Layout of Data Acquisition.

1–3 m range. The system maintained stable operation (CPU utilization ≤ 15 % on our i7-10750H test platform) throughout the stress tests.

4.2. Basic Working scenario

To precisely assess breathing patterns, we conducted extensive experiments in a controlled laboratory setting, as illustrated in Fig. 5; ten participants were directed to breathe at irregular rates, as indicated in Table 3, detailing each subject's characteristics. While our study included participants with a range of heights (139–177 cm), weights (125–180 lbs), and ages (20–36 years), future work should expand the diversity of the dataset to include a broader demographic representation, including different age groups, body types, and potential respiratory conditions. Additionally, testing in various environments beyond controlled laboratory settings would further validate the – robustness of the system. Each participant signed a consent form prior to participating in the study. Our complete dataset comprised 420 experimental trials (10 participants × 3 breathing patterns × 14 scenario combinations), with each 30-second trial sampled at 20 Hz yielding 600 data points. The dataset was carefully partitioned using participant-wise stratification to ensure fair representation across all subsets.Prior to the experiments, all subjects were directed to view publicly available YouTube videos illustrating various abnormal respiratory patterns and practice replicating these patterns based on their unique features and clinically plausible respiratory rates. The use of simulated patients (healthy individuals trained to emulate patient conditions) is prevalent in medical education and essential for understanding illnesses. We acknowledge that our use of simulated patients, although common in medical research [44], may not capture all nuances of genuine respiratory abnormalities, and clinical trials with actual patients would be valuable for further validation. Future clinical trials involving actual patients are essential for complete validation.

Consequently, testing and validating the proposed system with simulated abnormal breathing patterns is a pivotal step towards clinical trials and real-world applications. Each participant was directed to breath at eupnea denoted by 'E,' bradypnea denoted by 'B,' and tachypnea rates denoted by 'T' for individual scenarios, resulting in three distinct cases, highlighting the study's comprehensive approach to evaluating varied respiratory patterns. In two-person scenarios, both individuals breathed at eupnea, bradypnea, and tachypnea rates, leading to six potential scenarios; Similarly, scenarios with three, four, and five participants, where each breath at these varying rates resulted in seven, twelve, and eleven potential cases, respectively, demonstrated a thorough examination of respiratory patterns across different group sizes. Each 30-second activity was conducted with general trials to ensure high accuracy. Fig. 6. highlights all multi-person scenarios, emphasizing a meticulous approach for obtaining reliable results.

5. Results and Discussion

The remainder of this paper is organized as follows: Section V-A focuses on measuring respiratory rates in both individual and group scenarios by analyzing various cases using time- and frequency-domain CSI amplitude data. Section V-B applies machine-learning algorithms to classify these respiratory rates, providing a comprehensive interpretation and evaluation of the results for both individual and group scenarios.

5.1. Respiratory rate measurement

In this section, the respiratory rates are measured using CSI amplitude data in both the time and frequency domains, as elaborated below.

5.1.1. Time domain CSI amplitude analysis for multi-person respiratory rate Measurement

In this section, the accurate extraction of respiratory rates from time-domain CSI amplitude data presents significant challenges, particularly in multi-person scenarios. Although the cycle count in CSI signals can be directly correlated with the respiratory rate in single-person cases, simultaneous chest movements in multi-person environments lead to overlapping CSI amplitude variations. These interferences complicate the isolation of individual respiratory rates, thereby requiring advanced signal separation techniques. In this study, we addressed these complexities by employing Blind Source Separation (BSS) [45,46], Independent Component Analysis (ICA) [43], and adaptive filtering to disentangle and process overlapping signals effectively.

Respiratory rates were categorized into three types: Eupneic (EUP), Bradypneic (BRD), and Tachypneic (TAC). The detailed analyses were conducted for single-person, dual-person, triple-person, quad-person, and quint-person cases, as illustrated in Fig. 7(a-e).

Fig. 7 shows the separated respiratory signals after BSS/ICA processing. While minor temporal misalignments are visible (due to independent component extraction), they are resolved in frequency-domain analysis and do not impact classification accuracy.

The slight misalignment in the curves arises from the natural variability in individual respiratory cycles. Each subject's breathing cycle is independent, leading to slight offsets in the timing of their breaths. Despite this, all subjects were breathing simultaneously. The misalignment does not affect the system's ability to accurately classify the respiratory patterns, as confirmed by the robust classification performance. This explanation has been included in the figure caption for further clarity.Fig. 7a. demonstrates the results of the single-person analysis, where the respiratory rate was derived by counting the cycles in the CSI amplitude over a 30-second period. We observed 18 cycles, corresponding to a respiratory rate of 13 bpm, which falls within the EUP range. In this scenario, the traditional time-domain analysis was sufficient because there were no overlapping signals.

In Fig. 7b, the dual-person analysis is illustrated, where overlapping BRD and TAC patterns resulted in significant signal interference. The CSI amplitude variations from the two individuals interfered with each other, making it difficult to differentiate the respiratory rates using basic time-domain methods. To address this, the BSS was applied, configured

E	B	T	EEEEE	BBBBB	TTTTT	ONE PERSON
EE	BB	TT	EEBBT	BBTTE	EEEBT	TWO PERSON
EB	ET	BT	BBBET	TTTEB	EBTEE	THREE PERSON
EEEE	BBBB	TTTT	EBTBB	EBTET	EBT	FOUR PERSON
EEBB	EETT	BBTT	EEE	BBB	TTT	FIVE PERSON
EEEB	BBBE	TTTE	EEB	BBE	TTE	
EBTE	EBTB	EBTT				

Fig. 6. Cases for multi person scenarios.

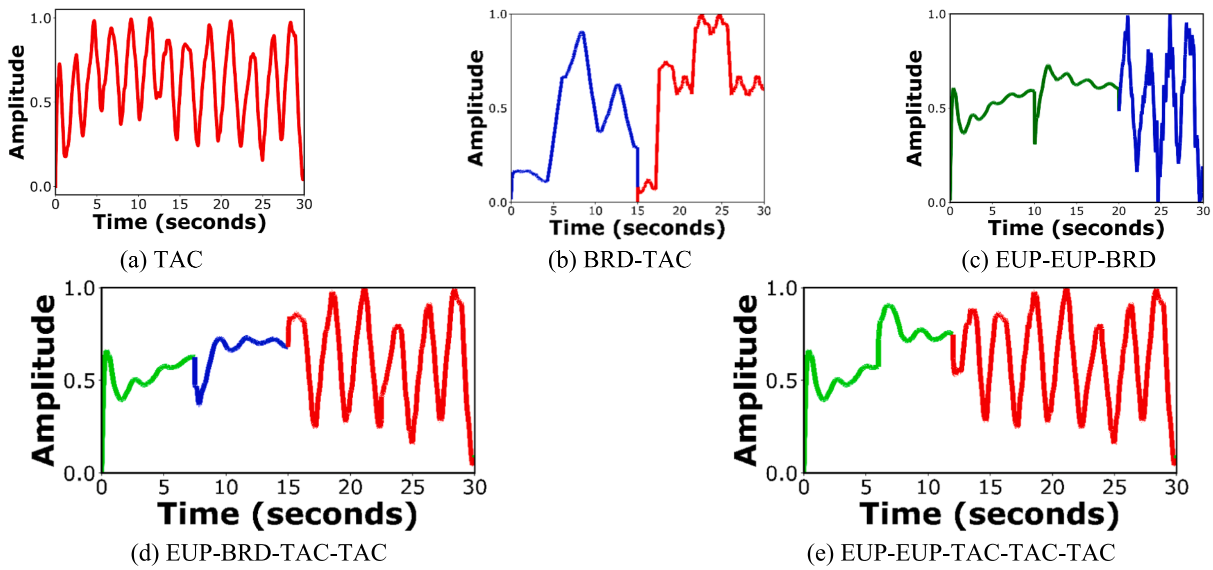

Fig. 7. Time-domain CSI amplitude signals after BSS/ICA separation: (a) Single-person tachypnea (TAC), (b) Dual-person bradypnea-tachypnea (BRD-TAC) using BSS, (c) Triple-person (EUP-EUP-BRD) with adaptive filtering, (d) Quad-person (EUP-BRD-TAC-TAC), (e) Quint-person (EUP-EUP-TAC-TAC-TAC).

with a 3-second window, to accurately isolate the independent signals corresponding to each individual's chest movements. This precisely discriminated the BRD pattern from the TAC pattern, demonstrating the capability and accuracy of the BSS in separating overlapping signals in multi-person analysis.

In the more complex scenario of the triple-person analysis, as illustrated in Fig. 7c, three distinct respiratory patterns—EUP, BRD, and TAC—were identified. In this analysis, BSS, in conjunction with adaptive filtering, was employed to distinguish and accurately resolve each individual's respiratory rate. The adaptive filtering technique employs a dynamically adjustable windowing method, that adapts the filter coefficients every 2 s based on the signal characteristics. This approach significantly reduces noise and minimizes signal interference caused by simultaneous chest movements. The combination of BSS and adaptive filtering enabled the precise extraction of each individual's respiratory rate, despite the challenges posed by the overlapping variations in the CSI amplitude variations.

As shown in Fig. 7d, four individuals with EUP, BRD, and TAC patterns were analyzed. ICA was integrated with BSS to improve signal separation. With a 5-second window, ICA effectively identified independent respiratory signals from the mixed CSI data, distinguishing four distinct breathing patterns by utilizing the statistical properties of the signals. The combined use of BSS, ICA, and adaptive filtering enabled the precise and clear separation of each respiratory cycle, even in this more complex multi-person scenario.

Finally, In the quint-person analysis, depicted in Fig. 7e, posed significant challenges owing to the extensive overlap in the CSI signals from five individuals. To overcome this, BSS, ICA, and adaptive filtering were sequentially applied.The BSS, using a 4-second sliding window, captured the dynamic variations in the mixed signals. Subsequently, ICA was applied with a 5-second window to further differentiate the independent components, relying on statistical properties, including non-Gaussianity and signal independence. This process was particularly effective in disentangling complex overlaps, where the BSS alone struggled.

To further refine the signals, adaptive filtering was employed with a 2-second coefficient adjustment interval to reduce noise and enhance clarity. This combination of methods enabled the accurate classification of three EUP and two TAC breathing patterns, demonstrating the robustness and precision of the approach in multi-person scenarios with overlapping signals.

5.1.2. Frequency domain CSI amplitude analysis for multi-person respiratory rate Measurement

In this section, frequency-domain CSI data are used to measure the respiratory rates in a multi-person analysis. The study examined three cases, ranging from a single-person to a quint-person scenario, with FFT applied for frequency-domain analysis. This method enables precise extraction of respiratory patterns, allowing for the accurate detection of multiple subjects across varying complexities.

For the one-person analysis, see Fig. 8(a-c). shows the system analysis of a single subject, where clear frequency peaks corresponding to EUP (0.23 Hz), BRD (0.18 Hz), and TAC (0.45 Hz) were identified. Through frequency transformation, the system effectively distinguished between different respiratory patterns, providing a detailed view of the individual breathing behavior. A representative example in Fig. 8c demonstrates the proposed classification protocol. While the 0.1–0.2 Hz bin shows maximum raw PSD (0.92), it is rejected as: (1) its second harmonic at 0.45 Hz better matches the tachypnea range (24 bpm = 0.4 Hz), and (2) its power ratio (0.1 Hz/0.45 Hz = 0.28) indicates harmonic interference. The 0.4–0.45 Hz bin is selected despite lower raw PSD (0.81) due to its clinical validity and absence of higher harmonics (0.45 Hz/0.9 Hz ratio $<$ 0.1).In the dual-person analysis, illustrated in Fig. 9 (a-b), the ability to isolate distinct respiratory frequencies at 0.22 Hz and 0.45 Hz demonstrates the system's capacity to differentiate between individuals, even when they are breathing at different rates. The separation of signals was precise, highlighting the system's capability to handle multi-person scenarios with ease. Fig. 10(a-b). introduces three subjects with varying breathing rates. The detection of three well-separated peaks at 0.19 Hz, 0.23 Hz, and 0.48 Hz shows the robustness of the system robustness in distinguishing multiple signals in more complex scenarios.

In Fig. 11(a-b), four distinct respiratory rates are detected, with peaks ranging from 0.18 Hz to 0.45 Hz. This figure illustrates the continued accuracy of the system as the number of subjects increases, maintaining clear signal separation and high resolution despite the growing complexity.

Finally, Fig. 12(a-b) demonstrates the system's capability to resolve five simultaneous respiratory patterns, where each peak corresponds to a distinct rate (e.g., 0.18 Hz BRD, 0.45 Hz TAC) from the pre-assigned subjects described in Table 3. While the system isolates these patterns with precision, it relies on controlled experimental conditions in which the subjects maintain fixed positions and breathing rates. In

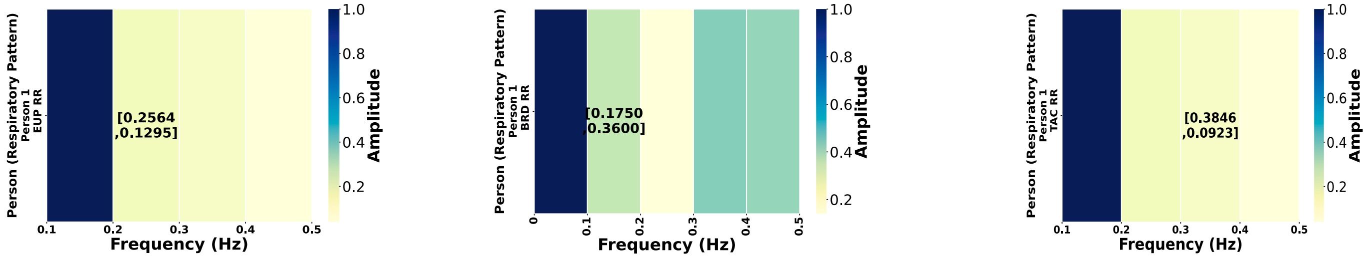

(a) EUP (b) BRD (c) TAC

Fig. 8. One-person respiratory rate classification.

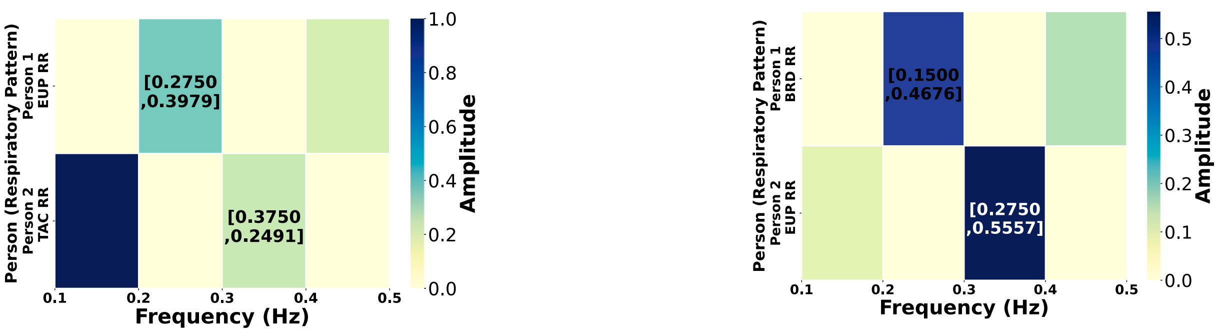

(b) EUP-TAC (c) BRD-TAC

Fig. 9. Two-person respiratory rate classification.

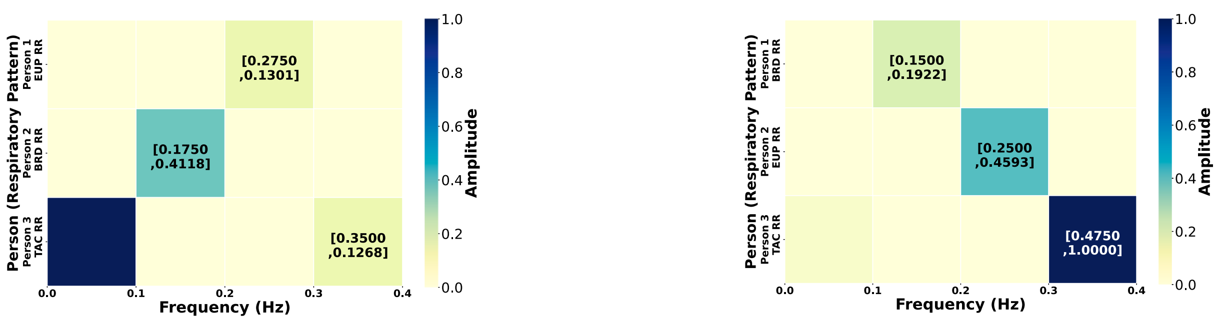

(a) EUP-BRD-TAC (b) BRD-EUP-TAC

Fig. 10. Triple-person respiratory rate classification.

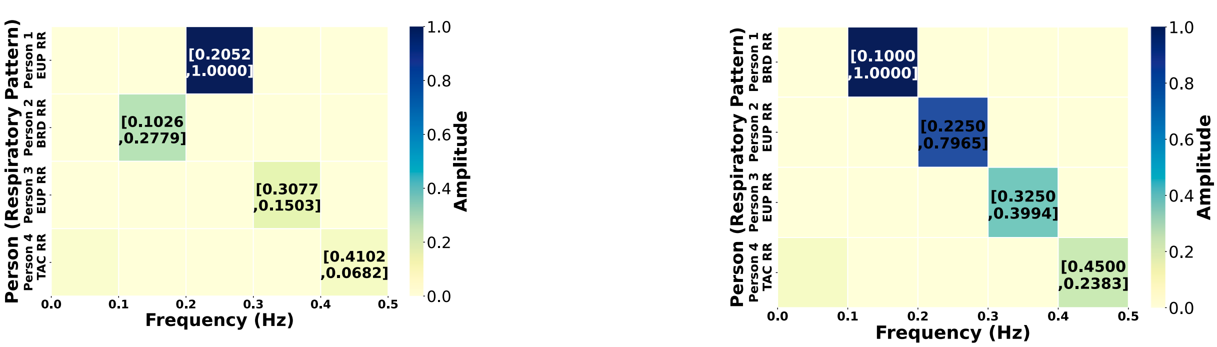

(a) EUP-BRD-EUP-TAC (b) BRD-EUP- EUP-TAC

Fig. 11. Quad-person respiratory rate classification.

uncontrolled environments, additional spatial or biometric data (e.g., antenna arrays for user localization) are required to associate patterns with specific individuals. In Figs. 8-12, the two numbers in square brackets represent the horizontal frequency (in Hz) and the vertical power spectral density (PSD) at that frequency (in arbitrary units). The frequency values are derived from FFT analysis of the respiratory signals, and the PSD indicates the intensity of the signal at each frequency.

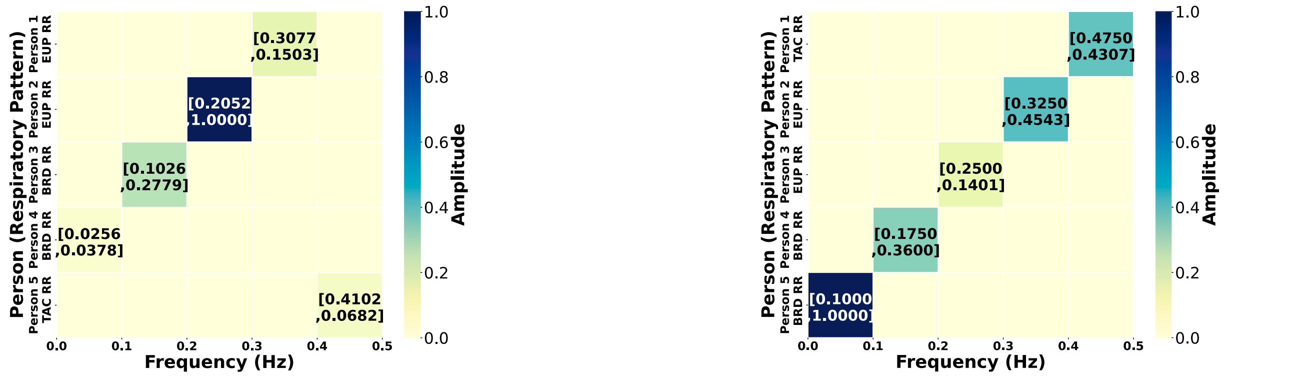

(a) EUP-EUP-BRD-BRD-TAC (b) TAC-EUP-EUP-BRD-BRD

Fig. 12. Quint-person respiratory rate classification. *Note for* Figs. 8–12*:* Normalized power spectral density (PSD) shown in 0.05 Hz bins (color intensity scale: 0–1). Final classifications (marked ▢) exclude harmonic artifacts using the validation criteria defined in Section 3.2.4 (peak detection threshold: 85th percentile; harmonic rejection: power ratio < 0.3).

5.2. Respiratory rate rate classification

In this section, various machine learning algorithms—Medium Tree, Linear Discriminant, Naive Bayes, Linear SVM, and Coarse KNN—are used to classify respiratory rates in multi-person scenarios. Cross-validation (CV) was employed to ensure a robust evaluation. This technique assesses data by generating predictions from data that were not used during training. The dataset was divided into subsets for training and testing, with the CV method ensuring a comprehensive evaluation. The Medium Tree algorithm was selected after extensive comparative evaluation because of its optimal balance between accuracy and computational efficiency, which is particularly important for real-time applications. It achieved superior performance (AUROC scores of 98.5 % to 89.8 % across scenarios) while maintaining reasonable training durations (69.4 s for single-person to 13.6 s for quint-person cases). Hyperparameter optimization was conducted using Bayesian optimization with 5-fold cross-validation, focusing on maximum tree depth (optimized to 20), minimum leaf size (optimized to 8), and split criterion (Gini's diversity index).Although ensemble methods (e.g., Random Forest) and deep learning approaches showed comparable accuracy in preliminary tests, their significantly higher computational requirements made them less suitable for real-time deployment with current hardware constraints. The Medium Tree algorithm was chosen for its balance of accuracy and computational efficiency, particularly in multi-subject scenarios. It consistently outperformed the other models in terms of the accuracy prediction rate, and training duration, making it the primary model in this study. The linear Discriminant and Naive Bayes were selected for their efficiency and simplicity, serving as strong baselines for comparison. Linear SVM and Coarse KNN were included for their robustness in handling complex datasets, though they require more computational resources.

1) Single-Person Analysis: There cases were considered for the single-person analysis, as shown in Table 4. Five ML algorithms were evaluated, and their performances were detailed. As illustrated in Table 5, the Medium-Tree model demonstrated the highest precision, achieving an accuracy of 98.5 %.

2) Dual-Person Analysis: Six cases were considered for dual-person analysis, as shown in Table 6. Five ML algorithms were evaluated, and their performances are presented in Table 7, with the Medium Tree algorithm achieving the highest accuracy of 97.9 %.

3) Triple-Person Analysis: For the triple-person analysis, seven cases were considered, as shown in Table 8. Five ML algorithms were evaluated, and their performance is presented in Table 9. The medium-tree algorithm achieved an accuracy of 94.9 %.

4) Quad-Person Analysis: For the quad-person analysis, twelve cases are considered, as shown in Table 10. Five ML algorithms are evaluated, and their performance is shown in Table 11. The Medium-Tree algorithm achieved a maximum accuracy of 91.8 %.

5) Quint-Person Analysis: For the quint-person analysis, eleven cases are considered, as shown in Table 12. Five ML algorithms were evaluated, and their performance is presented in Table 13, with the Medium Tree algorithm achieving a maximum accuracy of 89.8 %.Our comparative analysis of machine learning algorithms as shown in Table 14 reveals that while advanced methods like Random Forest (97.8 % accuracy) and SVM-RBF (98.1 %) achieve marginally better single-subject classification than our Medium Tree (97.5 %), they require 3.2–4 × more computation time (1200–950 vs. 3800 obs/sec). More critically, in multi-subject scenarios – the primary focus of clinical deployment – the Medium Tree outperforms all alternatives by 1.3–7.4 percentage points (89.8 % accuracy with five subjects) while maintaining superior computational efficiency (2.8–5.8 × faster inference,

Table 5
Evaluation of ML Algorithms Performance for Single-Subject Analysis.

Model	Performance (%)	Prediction rate (obs/sec)	Training duration (s)
Medium Tree	98.5	~3800	69.4
Linear Discriminant	94.6	~2700	52.2
Naive Bayes	98.3	~990	99.3
Linear SVM	97.4	~4600	97.8
Coarse KNN	96.4	~3200	90.5

Table 4
Class Label Classification for Single-Subject Analysis.

Class Label	Individual 1
I	EUP
II	BRD
III	TAC

Table 6
Class Label Classification for Dual-Subject Analysis.

Class Label	Individual 1	Individual 2
I	EUP	EUP
II	BRD	BRD
III	TAC	TAC
IV	EUP	BRD
V	EUP	TAC
VI	BRD	TAC

Table 7
Evaluation of ML Algorithms Performance for Dual-Person Analysis.

Model	Performance (%)	Prediction rate (obs/sec)	Training duration (s)
Medium Tree	97.9	32,000	8.2
Linear Discriminant	96.3	29,000	10.4
Naive Bayes	96.2	820	20.8
Linear SVM	97.7	4300	12.9
Coarse KNN	94.2	7500	10.2

Table 8
Class Label Classification for Triple-Subject Analysis.

Class Label	Individual 1	Individual 2	Individual 3
I	EUP	EUP	EUP
II	BRD	BRD	BRD
III	TAC	TAC	TAC
IV	EUP	EUP	BRD
V	BRD	BRD	EUP
VI	TAC	TAC	EUP
VII	EUP	BRD	TAC

Table 9
Evaluation of ML Algorithms Performance for Triple-Person Analysis.

Model	Performance (%)	Prediction rate (obs/sec)	Training duration (s)
Medium Tree	94.9	9600	20.8
Linear Discriminant	93.6	7500	71.8
Naive Bayes	92.9	930	68.2
Linear SVM	93.9	9600	66.9
Coarse KNN	94.3	7000	62.0

Table 10
Class Label Classification for Quad-Subject Analysis.

Class Label	Individual 1	Individual 2	Individual 3	Individual 4
I	EUP	EUP	EUP	EUP
II	BRD	BRD	BRD	BRD
III	TAC	TAC	TAC	TAC
IV	EUP	EUP	EUP	BRD
V	EUP	EUP	BRD	BRD
VI	EUP	BRD	TAC	TAC
VII	EUP	BRD	TAC	EUP
VIII	EUP	BRD	TAC	BRD
IX	BRD	BRD	TAC	TAC
X	BRD	BRD	BRD	EUP
XI	TAC	TAC	TAC	EUP
XII	EUP	EUP	TAC	TAC

Table 11
Evaluation of ML Algorithms Performance for Quad-Person Analysis.

Model	Performance (%)	Prediction rate (obs/sec)	Training duration(s)
Medium Tree	91.8	35,000	11.6
Linear Discriminant	91.1	43,000	18.9
Naive Bayes	90.5	680	40.2
Linear SVM	88.3	5000	25.7
Coarse KNN	89.9	7000	45.4

2.1–3.3 × lower memory usage). These results demonstrate that simpler architectures can better balance accuracy and real-time performance for respiratory monitoring applications.

The performance of these algorithms, evaluated using the AUROC metric with the one-vs-rest strategy, varied across scenarios and was verified through cross-validation for consistent accuracy [44]. A paired *t*-test evaluated statistical significance, with the Medium Tree model

Table 12
Class Label Classification for Quint-Subject Analysis.

Class Label	Individual 1	Individual 2	Individual 3	Individual 4	Individual 5
I	EUP	EUP	EUP	EUP	EUP
II	EUP	EUP	EUP	BRD	TAC
III	EUP	EUP	BRD	BRD	TAC
IV	EUP	BRD	TAC	EUP	TAC
V	EUP	BRD	TAC	EUP	EUP
VI	EUP	BRD	TAC	BRD	BRD
VII	BRD	BRD	TAC	TAC	EUP
VIII	BRD	BRD	BRD	EUP	TAC
IX	BRD	BRD	BRD	BRD	BRD
X	TAC	TAC	TAC	TAC	TAC
XI	TAC	TAC	TAC	EUP	BRD

Table 13
Evaluation of ML Algorithms Performance for Quint Person Analysis.

Model	Performance (%)	Prediction rate (obs/sec)	Training duration(s)
Medium Tree	89.8	10,000	13.6
Linear Discriminant	87.6	62,000	12.9
Naive Bayes	86.7	730	29.7
Linear SVM	85.3	5000	19.1
Coarse KNN	83.9	12,000	34.7

Table 14
Comparative Performance of Machine Learning Algorithms with state of the art for Respiratory Pattern Classification.

Model	Accuracy(1-subject)	Accuracy(5-subject)	Inference Speed (obs/sec)	Training time (s)
Medium Tree	97.5 %	89.8 %	3800	69.4
Random Forest	97.8 %	87.2 %	1200	142.1
SVM-RBF	98.1 %	83.7 %	950	185.6
XGBoost	97.6 %	88.5 %	2100	98.3
MLP	96.9 %	82.4 %	650	230.5

achieving the highest AUROC scores across all scenarios: 98.5 % for single-subject, 97.9 % for dual, 94.9 % for triple, 91.8 % for quad, and 89.8 % for quint-subject classification.The AUROC of the Linear Discriminant model ranged from 94.6 % to 87.6 %,while that of the Linear SVM achieved 97.4 % to 85.3 %. Naive Bayes and Coarse KNN started with high AUROC for single subjects (98.3 % and 96.4 %, respectively) but declined in quint-subject cases. A paired *t*-test revealed a p-value of 0.0238, indicating that the Medium Tree model significantly outperformed the Linear Discriminant model, confirming its robustness for complex multi-class classification. These findings highlight the need to choose the correct model based on the dataset characteristics and task demands, as shown in Fig. 13.

5.2.1. *Computational performance analysis*

The computational requirements of the system were carefully evaluated to determine real-time feasibility. Using an Intel Core i7-10750H processor with 16 GB RAM, the Medium Tree classifier achieved prediction rates ranging from ∼ 3800 observations/second (single-person) to ∼ 10000 observations/second (quint-person), which is sufficient for real-time monitoring at 20 Hz sampling.The training times varied from 69.4 s (single-person) to 13.6 s (quint-person), which is acceptable for periodic model updates. The USRP hardware operates with a 20 MHz bandwidth at 400MS/s, requiring approximately 15 % CPU utilization during continuous monitoring.

Table 15
Comparative Evaluation of Respiratory Pattern Monitoring Techniques.

Study	Technology & Approach	Features & Techniques	Accuracy & Validation	Advantages/Limitations
[26]	Wi-Fi CSI, Deep Learning	Wi-Fi-based breathing pattern recognition	Not specified/Deep learning validation (1 person)	Non-contact, widely available signals. / noise-sensitive
[48]	WiFi CSI, Domain Adaptation	WiFi CSI, Domain Adaptation	1 subject	Uses existing infrastructure/Low multi-person scalability
[29]	2.4-GHz Doppler Radar, SVM	Six breathing patterns classification, Doppler shift analysis	94.7 %/SVM modelEvaluation (1 person)	High accuracy for single person. /Hardware-specific (Doppler radar)
[30]	UWB Radar, 1D CNN	Deep learning-based classification of four breathing rhythms	95.8 %/Cross-validation (1 person)	Precise pattern recognition/ Resource intensive for real-time use
[39]	Sub-6 GHz SDR, Micro-Doppler Radar	Separation of heartbeat and respiratory signals using radar	Not specified/ Micro-Doppler signal analysis	High precision/Complex setup and calibration
[47]	IR-UWB Radar, Random Forest	Random Forest classification of four distinct respiration patterns	90 %/Random Forestperformance (1 person)	High accuracy using traditional ML. /Single-person focused
[49]	Thermal & Visible Imaging	Thermal & visible imaging for multi-person monitoring	Not specified/Model tested in various scenarios	Multi-person visual monitoring. / light-sensitive
[50]	Infrared Thermography, CNN	Thermal imaging for apnea detection	1 subject	No RF interference/Lighting-dependent
This work	**SDR with RF Sensing, Machine Learning**	**Multi-person detection, AUROC analysis, Medium Tree classifier**	**98.5 % (1 person),89.8 % (5 persons) /AUROC, p-test**	**Real-time, multi-person monitoring**

For clarity, the bold text highlights the outcomes achieved in this study.

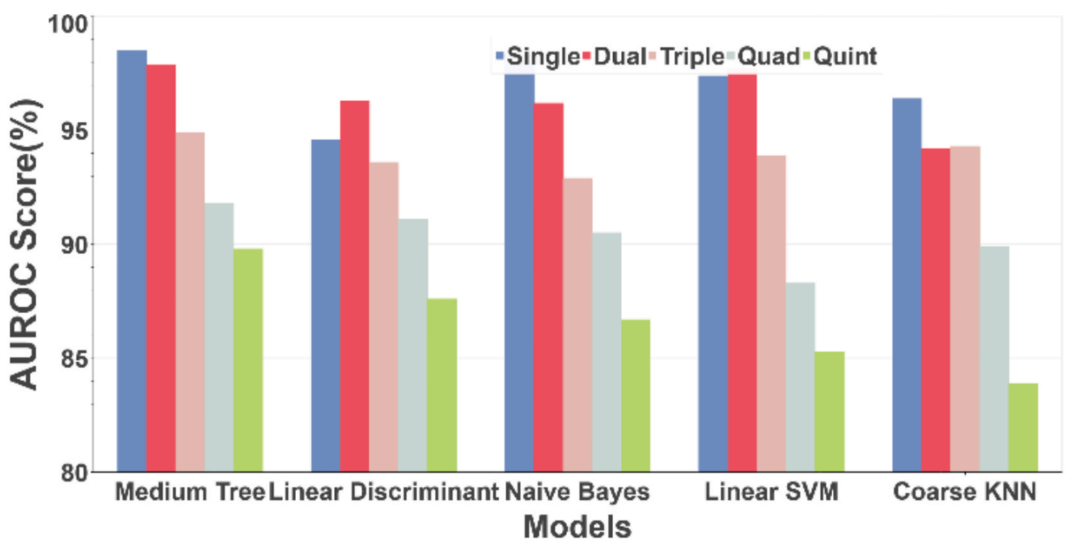

Fig. 13. The Comparison of AUROC scores for Medium Tree, Linear Discriminant, Naive Bayes, Linear SVM, and Coarse KNN classifiers across 1–5 subjects.

5.3. Comparative EVALUATION with other significant research

Table 15. compares breathing pattern monitoring methods, highlighting differences in technology, techniques, and performance. Our SDR-based system with RF sensing and a Medium Tree classifier achieved 98.5 % accuracy for one person and 89.8 % accuracy for five persons, validated via AUROC and p-test. Unlike [29] Doppler Radar (94.7 %) and [30] UWB Radar with 1D CNN (95.8 %), our system enables real-time, multi-person monitoring with lower computational demand [26,47] use Random Forest and Wi-Fi CSI deep learning, focusing on single-person detection and environmental sensitivity. The domain adaptation approach in WiFi CSI [48] improves generalizability across body types but is fundamentally limited to individual monitoring scenarios. Alternative modalities such as [49,50] thermal imaging and [39] Sub-6 GHz Micro-Doppler Radar offer alternatives but face limitations in setup and lighting. Our approach balances accuracy, scalability, and cost-effectiveness, offering a robust, integrated solution for scalable real-world respiratory monitoring applications.

6. Conclusions

This study presents the development of an RF-sensing-based SDR system designed for continuous monitoring of respiratory rates in domestic environments. The system effectively detected EUP, BRD, and TAC respiratory rates in multi-person scenarios, accommodating up to five individuals at a time. The system demonstrated promising scalability for monitoring up to five individuals simultaneously, although the accuracy decreased as the group size increased (from 98.5 % for single-person to 89.8 % for five-person scenarios). For larger groups, potential solutions could include: (1) deploying multiple synchronized SDR units with spatial diversity, (2) implementing advanced signal separation techniques like deep learning-based blind source separation, and (3) optimizing computational efficiency through hardware acceleration. Real-world deployment would benefit from adaptive algorithms that can handle dynamic environments with moving subjects, which represents an important direction for future research. Initially, FFT-based methods were employed to detect the respiratory rates of multiple persons, followed by the use of various ML algorithms for their classification. Among the ML algorithms tested, the Medium Tree algorithm demonstrated the highest accuracy for classifying respiratory rates across different multi-person scenarios, achieving a peak accuracy of 98.5 % for the single-person scenario. However, a gradual decrease in the accuracy was observed as the number of individuals increased. Future work may involve further optimizing these models or exploring additional features to improve both accuracy and prediction speed. However, a gradual decrease in the accuracy was observed as the number of individuals increased.

Despite these promising results, this study has several limitations. Although useful, the dataset may not be sufficiently large or diverse to ensure generalisability to all real-world scenarios of this study. The potential imbalance in class distributions (EUP, BRD, and TAC) could lead to biased model performance, favoring more frequent classes over less frequent classes. Additionally, the increasing complexity with more persons introduces scalability challenges, as the accuracy tends to decrease. The computational resources required for training and prediction, particularly for more complex models, such as the Medium Tree, may also be substantial.

Furthermore, this system has only been tested in a static indoor environment, ignoring large-scale movements. While our controlled experiments establish strong baseline performance, we recognize the need for future validation in truly unconstrained environments with untrained subjects and variable participant counts. Real-world applications would require testing in dynamic environments with walking or falling subjects, which may introduce additional challenges for signal processing and classification. This study relied on a limited set of features, potentially missing important aspects of the respiratory patterns. Moreover, while various algorithms were tested, hyperparameter tuning might not be exhaustive, potentially leaving some performance improvements unexplored. Finally, the specific scenarios tested (one-person, two-person, etc.) may not cover all possible configurations, limiting the external validity of the results.

CRediT authorship contribution statement

Malik Muhammad Arslan: Writing – original draft. **Xiaodong Yang:** Project administration, Funding acquisition. **Lei Guan:** Investigation. **Nan Zhao:** Investigation. **Tao Cui:** Investigation. **Mubashir Rehman:** Writing – review & editing, Conceptualization. **Abbas Ali Shah:** Investigation. **Muhammad Bilal Khan:** Supervision, Investigation, Conceptualization. **Syed Aziz Shah:** Supervision. **Qammer H. Abbasi:** Supervision.

Declaration of competing interest

The authors declare that they have no known competing financial interests or personal relationships that could have appeared to influence the work reported in this paper.

Acknowledgements

This work was supported by National Natural Science Foundation of China (No. 62201413 and 61671349).

Data availability

The authors do not have permission to share data.

References

[1] A.C. Guyton, Text book of medical physiology. China, 2006.
[2] M.A. Cretikos, R. Bellomo, K. Hillman, J. Chen, S. Finfer, A. Flabouris, Respiratory rate: the neglected vital sign, Med. J. Aust. 188 (11) (2008) 657–659.
[3] J.E. Hall, M.E. Hall, *Guyton and hall textbook of medical physiology e-book: Guyton and hall textbook of medical physiology E-Book*, Elsevier Health Sci. (2020).
[4] M. Javorka, et al., Role of respiration in the cardiovascular response to orthostatic and mental stress, American Journal of Physiology-Regulatory, Integrative and Comparative Physiology 314 (6) (2018) R761–R769.
[5] W.-M. Liang, et al., Respiratory patterns and physical fitness in healthy adults: a cross-sectional study, BMC Public Health 24 (1) (2024) 228.
[6] C. Chourpiliadis, A. Bhardwaj, Physiology, Respiratory Rate (2019).
[7] F. Depta, et al., Determining respiratory rate using measured expiratory time constant: a prospective observational study, J. Crit. Care 73 (2023) 154174.
[8] H. Pysick, S. Bowmaster, B. Gehlbach, and K. Doerschug, "Gasping, Bradypnea, and Obtundation: An Unusual Case of Respiratory Failure From Seizures," in B80-4. THE Z-files of sleep puzzles: American Thoracic Society, 2024, pp. A4580-A4580.
[9] S.B. Park, D. Khattar, "Tachypnea," in *StatPearls [internet]*, StatPearls Publishing (2024).
[10] Y. Wang, et al., Unobtrusive and automatic classification of multiple people's abnormal respiratory patterns in real time using deep neural network and depth camera, IEEE Internet Things J. 7 (9) (2020) 8559–8571.
[11] M.S. Badr, Central sleep breathing disorders: a critical evaluation of classification and diagnosis, Current sleep Medicine Reports (2024) 1–6.
[12] P.A. Lanfranchi, et al., Prognostic value of nocturnal Cheyne-Stokes respiration in chronic heart failure, Circulation 99 (11) (1999) 1435–1440.
[13] K.K. Dhatariya, N.S. Glaser, E. Codner, G.E. Umpierrez, Diabetic ketoacidosis, Nat. Rev. Dis. Primers 6 (1) (2020) 40.
[14] J. Phipps, et al., Early adverse physiological event detection using commercial wearables: challenges and opportunities, npj Digital Med. 7 (1) (2024) 136.
[15] P. Sharma, X. Hui, J. Zhou, T.B. Conroy, E.C. Kan, Wearable radio-frequency sensing of respiratory rate, respiratory volume, and heart rate, npj Digital Med. 3 (1) (2020) 98.
[16] U. Saeed, et al., Multiple participants' discrete activity recognition in a well-controlled environment using universal software radio peripheral wireless sensing, Sensors 22 (3) (2022) 809.
[17] B. Bujan, et al., Clinical validation of a contactless respiration rate monitor, Sci. Rep. 13 (1) (2023) 3480.
[18] M.M. Arslan, et al., Non-contact respiratory abnormality monitoring: a hybrid empirical mode and variational mode decomposition approach with software defined radio and deep learning, IEEE Sens. J. (2025).
[19] Z. Xu, et al., Simultaneous monitoring of multiple people's vital sign leveraging a single phased-MIMO radar, IEEE Journal of Electromagnetics, RF and Microwaves in Medicine and Biology 6 (3) (2022) 311–320.
[20] M. Ali, A. Elsayed, A. Mendez, Y. Savaria, M. Sawan, Contact and remote breathing rate monitoring techniques: a review, IEEE Sens. J. 21 (13) (2021) 14569–14586.
[21] F.-K. Wang, J.-X. Zhong, J.-Y. Shih, IQ signal demodulation for noncontact vital sign monitoring using a CW Doppler radar: a review, IEEE Journal of Electromagnetics, RF and Microwaves in Medicine and Biology 6 (4) (2022) 449–460.
[22] H. T. Yen, M. Kurosawa, T. Kirimoto, Y. Hakozaki, T. Matsui, and G. Sun, "Non-Contact Estimation of Cardiac Inter-Beat Interval and Heart Rate Variability Using Time-Frequency Domain Analysis for CW Radar," IEEE Journal of Electromagnetics, RF and Microwaves in Medicine and Biology, 2023.
[23] Y. Wang, et al., A novel non-contact respiration and heartbeat detection method using frequency-modulated continuous wave radar, IEEE Sens. J. (2024).
[24] W. Li, B. Tan, R.J. Piechocki, Wifi-based passive sensing system for human presence and activity event classification, IET Wireless Sens. Syst. 8 (6) (2018) 276–283.
[25] L. Guan, et al., Multi-person breathing detection with switching antenna array based on WiFi signal, IEEE Journal of Translational Engineering in Health and Medicine 11 (2022) 23–31.
[26] D. Fan, et al., A contactless breathing pattern recognition system using deep learning and WiFi Signal, IEEE Internet Things J. (2024).
[27] L. Maurya, P. Mahapatra, D. Chawla, Simultaneous breathing monitoring of multiple persons using thermal and visible imaging, IEEE Sens. J. 21 (24) (2021) 28057–28065.
[28] P. Sharma, Z. Zhang, T.B. Conroy, X. Hui, E.C. Kan, Attention detection by heartbeat and respiratory features from radio-frequency sensor, Sensors 22 (20) (2022) 8047.
[29] H. Zhao, et al., A noncontact breathing disorder recognition system using 2.4-GHz digital-IF Doppler radar, IEEE J. Biomed. Health Inform. 23 (1) (2018) 208–217.
[30] S.-H. Kim, Z.W. Geem, G.-T. Han, A novel human respiration pattern recognition using signals of ultra-wideband radar sensor, Sensors 19 (15) (2019) 3340.
[31] U. Saeed, et al., Wireless channel modelling for identifying six types of respiratory patterns with sdr sensing and deep multilayer perceptron, IEEE Sens. J. 21 (18) (2021) 20833–20840.
[32] S. He, Z. Han, C. Iglesias, V. Mehta, M. Bolic, A real-time respiration monitoring and classification system using a depth camera and radars, Front. Physiol. 13 (2022) 799621.
[33] Y. Ma, G. Zhou, S. Wang, WiFi sensing with channel state information: a survey, ACM Computing Surveys (CSUR) 52 (3) (2019) 1–36.
[34] M. Roopak, Y. Ran, X. Chen, G.Y. Tian, S. Parkinson, Channel state information based physical layer authentication for Wi-Fi sensing systems using deep learning in internet of things networks, IET Wireless Sens. Syst. (2024).
[35] Z. Guo, X. Zhu, L. Gui, B. Sheng, F. Xiao, BreathID: respiration sensing for human identification using commodity Wi-Fi, IEEE Syst. J. (2022).
[36] W. Xie, et al., A Real-time respiration monitoring system using WiFi sensing based on the concentric circle Model, IEEE Trans. Biomed. Circuits Syst. (2022).
[37] D. Huang, et al., Camera-based respiratory Imaging for intelligent rehabilitation assessment of thoracic surgery patients, IEEE Internet Things J. (2024).
[38] T.G. Troyee, M.M. Gani, M. Hasan, Design and implementation of low-cost respiratory rate measurement device, Arab. J. Sci. Eng. 49 (5) (2024) 6959–6969.

[39] C. Ma et al., "Noncontact Heartbeat and Respiratory Signal Separation Using a Sub 6 GHz SDR Micro-Doppler Radar," IEEE Journal of Electromagnetics, RF and Microwaves in Medicine and Biology, 2024.

[40] Y.-B. Tang and W.-C. Ge, "A novel OFDM symbol synchronization algorithm based on cyclic prefix in DVB-T," in 2008 4th International Conference on Wireless Communications, Networking and Mobile Computing, 2008: IEEE, pp. 1-4.

[41] Z. Wang, et al., A survey on CSI-based human behavior recognition in through-the-wall scenario, IEEE Access 7 (2019) 78772–78793.

[42] M. Rehman, et al., Development of an intelligent real-time multiperson respiratory illnesses sensing system using SDR technology, IEEE Sens. J. 22 (19) (2022) 18858–18869.

[43] R.M. Rangayyan, S. Krishnan, Biomedical signal analysis, John Wiley & Sons, 2024.

[44] H.S. Barrows, An overview of the uses of standardized patients for teaching and evaluating clinical skills, AAMC Acad. Med. 68 (6) (1993) 443–451.

[45] W. Zhang, et al., Broadband physical layer cognitive radio with an integrated photonic processor for blind source separation, Nat. Commun. 14 (1) (2023) 1107.

[46] Y. Wang, Y. Li, Q. Sun, Y. Li, A novel underdetermined blind source separation algorithm of frequency-hopping signals via time-frequency analysis, IEEE Trans. Circuits Syst. Express Briefs 70 (11) (2023) 4286–4290.

[47] D.-K.-H. Lai, et al., Dual ultra-wideband (UWB) radar-based sleep posture recognition system: Towards ubiquitous sleep monitoring, Eng. Regener. 4 (1) (2023) 36–43.

[48] Y. Zhang, F. Han, P. Yang, Y. Feng, Y. Yan, R. Guan, Wi-Cyclops: Room-scale WiFi sensing system for respiration detection based on single-antenna, ACM Trans. Sens. Netw. 20 (4) (2024) 1–24.

[49] L. Maurya, R. Zwiggelaar, D. Chawla, P. Mahapatra, Non-contact respiratory rate monitoring using thermal and visible imaging: a pilot study on neonates, J. Clin. Monit. Comput. 37 (3) (2023) 815–828.

[50] F. Gioia, F. Pura, A. Greco, D. Piga, A. Merla, M. Forgione, Contactless Estimation of respiratory Frequency using 3D-CNN on thermal Images, IEEE J. Biomed. Health Inform. (2025).